Atmos. Chem. Phys. Discuss., 14, 18389–18419, 2014
www.atmos-chem-phys-discuss.net/14/18389/2014/
doi:10.5194/acpd-14-18389-2014
© Author(s) 2014. CC Attribution 3.0 License.

Atmospheric Chemistry and Physics Discussions

This discussion paper is/has been under review for the journal Atmospheric Chemistry and Physics (ACP). Please refer to the corresponding final paper in ACP if available.

Characterisation of $J(O^1D)$ at Cape Grim 2000–2005

S. R. Wilson

Centre for Atmospheric Chemistry, School of Chemistry, University of Wollongong, NSW, Australia

Received: 16 May 2014 – Accepted: 20 June 2014 – Published: 10 July 2014

Correspondence to: S. R. Wilson (swilson@uow.edu.au)

Published by Copernicus Publications on behalf of the European Geosciences Union.

Abstract

Estimates of the rate of production of excited oxygen atoms due to the photolysis of ozone $J(O^1D)$ have been derived from radiation measurements carried out at Cape Grim, Tasmania (40.6° S, 144.7° E). These estimates agree well with measurements made during SOAPEX-II and with model estimates of clear sky photolysis rates. Observations spanning 2000–2005 have been used to quantify the impact of season, cloud and ozone column amount. The annual cycle of $J(O^1D)$ has been investigated via monthly means. These means show an inter-annual variation (monthly standard deviation) of 9 %, but in midsummer and midwinter this reduces to 3–4 %. Factors dependent upon solar zenith angle and satellite derived total ozone column explain 87 % of the observed signal variation of the individual measurements. The impact of total column ozone, expressed as a Radiation Amplification Factor (RAF), is found to be ~ 1.45, in agreement with model estimates. This ozone dependence explains 20 % of the variation observed at medium solar zenith angles (30–50°). The impact of clouds results in a median reduction of 14 % in $J(O^1D)$ for the same solar zenith angle range. At all solar zenith angles less than 50° approximately 10 % of measurements show enhanced $J(O^1D)$ due to cloud scattering and this fraction climbs to 25 % at higher solar angles. Including estimates of cloudiness derived from Long Wave Radiation measurements resulted in a statistically significant fit to observations but the quality of the fit did not increase significantly as measured by the reduced R^2.

1 Introduction

It is widely recognised that the chemistry of the clean troposphere is driven by a few key oxidizing species, with a major contributor being the hydroxyl radical (OH) (Crutzen, 1974). The hydroxyl radical reacts rapidly with a wide range of compounds, including methane, CO, and hydrocarbons. The concentration of OH present in the atmosphere is always small, but because of its high reactivity it can still play a dominant role in de-

ACPD
14, 18389–18419, 2014

termining the atmospheric fate of organics. It has also long been realised that changes in the amount of OH in the atmosphere could have a profound effect on global air quality and there has been a long-term effort to develop techniques to measure the key chemical species (Heard and Pilling, 2003). The most direct measure is the concentration of OH itself. There are several techniques now in use for such measurements, including fluorescence, UV absorption and mass spectrometry (Heard and Pilling, 2003) although none have been operated for long periods of time at a single site.

The primary source of OH is through the photolysis of ozone to produce $O(^1D)$ through the reactions:

$$O_3 + h\nu \xrightarrow{J(O^1D)} O(^1D) + O_2\left(^1\Delta_g, ^3\Sigma_g^-\right) \quad \text{(R1)}$$

$$O(^1D) + M \xrightarrow{k_2} O(^3P) \quad \text{(R2)}$$

$$O(^1D) + H_2O \xrightarrow{k_3} 2OH \quad \text{(R3)}$$

The branching ratio between Reactions (R2) and (R3) (Q) is given by:

$$Q = k_3[H_2O]/(k_3[H_2O] + \sum_i k_i[M_i]) \quad (1)$$

Here the summation is over the collision partners M_i, primarily O_2 and N_2. Q depends on the amount of water vapour, but typically around 10 % of $O(^1D)$ produced reacts to form OH ($Q \approx 0.1$). This can be calculated provided atmospheric pressure and the water vapour concentration is known, since the rate constants have been measured (Sander et al., 2006).

The rate of ozone photolysis in Reaction (R1), $J(O^1D)$, can be described by:

$$J(O^1D) = \int \sigma(\lambda,T)\phi(\lambda,T)F(\lambda)\mathrm{d}\lambda \quad (2)$$

which is the wavelength integration of $\sigma(\lambda,T)$, the (temperature dependent) absorption cross-section of ozone, $\phi(\lambda,T)$, the quantum yield of $O(^1D)$ production, and $F(\lambda)$, the

ACPD
14, 18389–18419, 2014

"actinic flux", which is the spherically integrated solar flux. There are a number of measurements of $J(O^1D)$ via chemical actinometers (Hofzumahaus et al., 2004), although due to their nature they are difficult to deploy for long periods of time, making either filter radiometers or spectral radiometers an attractive alternative (Bohn et al., 2008).

1.1 Techniques for the measurement of actinic flux (F)

There are a range of radiometric techniques used for the determination of actinic flux, and the strengths of various detectors has been assessed by a field comparison experiment (Bohn et al., 2008). All these techniques relied on calibrations using reference light sources.

1.1.1 Angular response

The ideal viewing geometry for the determination of $F(\lambda)$ detects photons from all directions equally (all 4π steradian). For locations not over reflective surfaces like snow the upwelling radiation is relatively small, and so most measurements of $F(\lambda)$ are made viewing down-welling radiation only (e.g., Junkermann et al., 1989).

Most quantitative UV observations measure global irradiance (E) (the energy striking a horizontal plane), and so there have been a number of attempts to convert global irradiance into actinic flux (Kazadzis et al., 2004; Kylling et al., 2003; McKenzie et al., 2002; Schallhart et al., 2004; Webb et al., 2002).

If it assumed that there is no upwelling radiation (surface albedo = 0), the actinic flux is given by

$$F = F_0 + F_{\downarrow} \tag{3}$$

where F_0 is the direct actinic flux and $F_{\downarrow}$ is the diffuse flux. Similarly, the global irradiance (E) is given by

$$E = \mu E_0 + E_{\downarrow} \tag{4}$$

ACPD
14, 18389–18419, 2014

where E_0 is now the direct beam irradiance, $\mu = \cos\theta$ where θ is the solar zenith angle and $E_\downarrow$ is the diffuse irradiance. As $E_0 = F_0$, it is now possible to simply write

$$F = \alpha E_\downarrow + E_0 \quad (5)$$

where α is the ratio of the diffuse actinic flux to diffuse irradiance. If the diffuse irradiance is not measured, this is recast in the form (Kazadzis et al., 2004)

$$\frac{F}{E} = \alpha + (1 - \alpha\mu)\frac{E_0}{E} \quad (6)$$

The ratio α is reasonably well behaved, especially at the wavelengths relevant for the $O(^1D)$ photolysis (McKenzie et al., 2002; Webb et al., 2002).

Estimating the ratio of the direct beam to global irradiance (E_0/E) has been more difficult. Schallhart et al. (2004) have therefore used a semi-empirical method which parameterized the relationship (F/E) based on the ratio of observed irradiance to clear sky irradiance, where the clear sky irradiance is calculated. Using data from four locations they found their results gave better agreement between measured and calculated F (7 %, 2σ) than that reported using Eq. (6) and no knowledge of the direct to global irradiance ratio (Kylling et al., 2003; Webb et al., 2002). Using global irradiance measurements combined with direct irradiance every 10 nm, Kazadzis et al. (2004) estimate an overall uncertainty of around 10 % (1σ).

1.1.2 Wavelength response

Three types of measurement detector have typically been used; a filter radiometer, a scanning spectrometer or a diode array/CCD detector equipped spectrometer system (Bohn et al., 2008; Hofzumahaus et al., 2004). Each approach has limitations. The filter radiometer measures at a fixed wavelength range, which needs then to be calibrated using the actual atmospheric ozone column and solar zenith angle factors (Bohn et al., 2004). The scanning spectrometer takes time to scan through the spectrum, rather

ACPD
14, 18389–18419, 2014

than measuring at a fixed time, leading to measures that are "time-smeared" rather than "time-averaged". For the production of a short-lived species like $O(^1D)$ this can lead to difficulties in comparing with other measurements. Finally, the diode array/CCD system needs to have well characterized stray-light corrections applied (Bohn et al., 2008; Hofzumahaus et al., 2004; Edwards and Monks, 2003).

1.2 Measurements of O^1D production at Cape Grim

The Cape Grim Baseline Air Pollution Station ("Cape Grim"), (40°40′56″ S, 144°41′18″ E) is a site near the northwest tip of Tasmania that experiences periods of clean maritime air from the southern ocean. During two intensive measurement campaigns SOAPEX-1 (1995) (Monks et al., 1998) and SOAPEX-2 (1999) (Creasey et al., 2003) filter radiometers have been deployed to measure $J(O^1D)$. During SOAPEX-2 the OH concentration was also measured. The measurements during the second campaign clearly demonstrated a simple link between $O(^1D)$ production and OH concentrations in clean atmosphere conditions (Creasey et al., 2003).

As part of the Cape Grim measurement program spectral UV-B irradiance (both global and diffuse) has been measured routinely. The purpose of this work is to use the spectral UV-B measurements to estimate $J(O^1D)$ for the period of SOAPEX-2 and 2000–2005, to assess estimates of the photolysis rates and to then develop a climatology. In particular, the impact of clouds and ozone will be assessed.

2 Experimental

All UV-B irradiance measurements reported here have been made in the radiation enclosure at the Cape Grim Baseline Air Pollution Station. This is located some 300 m north of the main building (Cainey et al., 2007). The location avoids the shadow of the telecommunication tower that is situated just to the north of the main building. The experimental details of the UV-B measurements and in-situ calibration technique have

ACPD
14, 18389–18419, 2014

been reported elsewhere (Wilson and Forgan, 1995; Wilson, 2006, 2007). In brief, the system alternately measures global and diffuse irradiance with a scanning double monochromator (Optronics Laboratories OL752) known as SRAD. Diffuse irradiance is measured by shading the global diffuser. The spectral scans are spaced at 5–10 min intervals, depending upon the time of day. The instrument is calibrated at 342 nm using well characterized sunphotometer measurements of direct beam irradiance, and the other wavelengths calibrated using the Ratio-Langley technique (Forgan, 1988). All this is referenced to a top of the atmosphere spectrum (Chance and Kurucz, 2010) which serves as the primary calibration of both wavelength and intensity. The optical input for the system was modified in October 1999, resulting in higher optical throughput (and hence better signal/noise ratios) and a diffuser with a better cosine response. Hence the period of operation during SOAPEX-2 (February 1999) is distinct from the period following the modification, although the measurement and calibration strategies are the same.

The resulting database of measurements includes alternative estimates of global and diffuse irradiance at each wavelength and time. The determination of the components of the irradiance at a single time is based on interpolation of the (e.g. diffuse) measurements before and after the (e.g. global) measurement in question (Wilson and Forgan, 1995), and so the derived signals are an approximation of the value for the 10–20 min period around the nominal measurement time.

The input diffuser was constructed from PTFE but was not temperature controlled. The phase change reported for this material at around 292 K (Ylianttila and Schreder, 2005) is therefore a source of uncertainty in these measurements. This will also impact upon the calibration, so that this will be at least partially captured in the variability of the calibrations.

ACPD
14, 18389–18419, 2014

3 Methodology

3.1 Derivation of $J(O^1D)$ production from UV-B measurements

As the Cape Grim UV data set includes both the diffuse and global irradiance, Eq. (5) can be used, as the direct beam irradiance can be derived from the difference between the global and diffuse (see Eq. 4). This leaves the determination of the ratio (α). For the wavelength region of interest (300–330 nm), a value of 2.0 could be used, which is the value appropriate for isotropic radiation (McKenzie et al., 2002). However, as the optical depth at Cape Grim is typically low (Wilson and Forgan, 2002), the calculated Rayleigh scattering values reported by Kylling et al. (2003) have been used to give a relationship:

$$\alpha = 2.01 - 0.052/\mu \quad (7)$$

In practice the difference between this and the isotropic assumption is small. For the ozone absorption cross section (σ (λ,T), Eq. 2) the measurements of Malicet et al. (1995) at 22 °C have been used, in conjunction with the temperature dependent O^1D quantum yield (Sander et al., 2006), derived using the hourly average air temperature measured at Cape Grim (as part of the meteorology program) (Cainey et al., 2007).

The UV-B measurements span the region 298–335 nm, and this can lead to an underestimate of the photolysis rate. A study by Jäkel et al. (2006) found that cut-offs below 298 nm did not perturb the estimate of $J(O^1D)$ by more than 5 %, with the maximum error at times of low column ozone and high sun. Test measurements using spectra measuring out to 340 nm found that including the region between 335–340 nm altered $J(O^1D)$ by less than 1 %. There is no recommended quantum yield for O^1D above 340 nm (Sander et al., 2006). The estimates presented here will therefore be biased low by the limited wavelength coverage by typically less than 5 %.

The calibration uncertainty of the measurements is estimated to be 5 % based on the uncertainties in the top of the atmosphere spectrum used as the calibration (Chance and Kurucz, 2010), and the variability in the calibration observed from the multiple

ACPD
14, 18389–18419, 2014

calibrations carried out during the 6 years, implying a total uncertainty of around 8 % in $F(\lambda)$. This does not include the impact of model assumptions including the assumption of isotropic diffuse irradiance.

3.2 Modeling $J(O^1D)$

In the analysis of data the model TUV version 5.0 has been used (Madronich and Flocke, 1997). One of the changes in this version of the model is the use of the same solar spectrum (Chance and Kurucz, 2010) as that used for the calibration of SRAD. The calculations have been run at a range of solar zenith angles using an aerosol optical depth of 0.05 at 550 nm, a value typical of conditions at Cape Grim (Wilson and Forgan, 2002).

4 Results and discussion

4.1 Comparison of measured $J(O^1D)$ with other measurements

During SOAPEX-2 there were two sets of filter radiometer measurements made covering a period of around 1 month (18 January 1999–17 February 1999). The filter radiometers were operated by a group from the University of Leicester and the University of Leeds (Sommariva et al., 2004). The radiometers are quoted as having an uncertainty of 20–30 % (Creasey et al., 2003; Monks et al., 1998; Sommariva et al., 2004) at solar zenith angles less than 60°. The filter radiometer values have been corrected for total ozone column and solar zenith angle dependence. A comparison of measurements as reported from SOAPEX-2 and SRAD are shown in Fig. 1. It can be seen that there is very good agreement between these two instruments under these conditions. It shows that the two estimation approaches, based on very different instruments and calibration strategies produce estimates of $J(O^1D)$ that are very similar.

A second comparison is the measurements with the clear sky calculations performed using TUV 5.0. The results of this are shown in Fig. 2. It can be seen that for the

ACPD
14, 18389–18419, 2014

data from both February 2000 (low column ozone) and October 2003 (high column ozone) there is good agreement between model and measurement (average deviation 2 %). Differences at high sun are around 3 %. Several days exist where the irradiance appears to vary smoothly but with differences of up to 10 % at solar noon. This could be due in part to the limited measurement range (Sect. 3.2), a calibration issue that occurs at these solar zenith angles, or due to cloud. The smooth change in $J(O^1D)$ implies no cloud near the sun, but there can be cloud well away from the sun that is reducing the observed photolysis rate. Without a measure of the cloud field it is hard to distinguish between these possibilities.

4.2 Annual cycle in $J(O^1D)$

The data collected for the period 2000–2005 are shown in Fig. 3. The dataset comprises of over 108 000 measurements. The gaps in the dataset represent times when the equipment failed.

The annual cycle is the dominant feature in this plot. To quantify this, monthly mean values have been calculated by sorting all data from a month into 24 hourly bins, and from these bins producing an average daily cycle for each month. It is assumed that if no measurement is made in one of the 24 hourly bins during the month that the average is zero, except where the hour before and after have non-zero values. In this case the average of those two values is used. This is only necessary where instrument failures have severely limited data collection in a particular month. The average of the 24 hourly averages is then calculated for each month in the 6 years. This method has been used to limit the impact of possible biases from collecting spectra at varying time intervals.

Despite the variability seen in the individual measurements (see Figs. 1 and 3), the monthly averages are relatively stable (Fig. 4, top panel). The lower panel of Fig. 4 shows that for mid-summer and mid-winter the interannual variability in the monthly averages is 3–4 %, with the increases in-between presumably driven by the rate of change of the solar zenith angle at midday, the factor also driving much of the observed

ACPD
14, 18389–18419, 2014

annual cycle. The resultant average monthly $J(O^1D)$ for Cape Grim is also presented in Table 1 along with the standard deviations.

Previous measurements of interannual variability of UV-B have been reported for Ushuaia in Argentina (Frederick et al., 2001). For global irradiance at 305 nm they found an interannual variability of around 25 %. The variability in global irradiance could be expected to be bigger than that for $J(O^1D)$ with the different dependence on the angle of incidence of radiation. The mean of the monthly relative standard deviation (9.2 %) is indeed slightly lower than that observed for global UV-B irradiance (10.8 %) as determined from the Cape Grim data. However, both are significantly less than reported from Argentina. This is presumably a reflection of the difference in climate, with Cape Grim routinely experiencing cloudy conditions.

To investigate any trend in the data both monthly trends for each month and trends as a function of season have been calculated. The most significant linear trend is in summer (December–February) (-1.7 ± 1.1 (std. dev.) % year^{-1}), but this is not significant at the 90 % level. Satellite estimates of changes in irradiance at 305 nm due to stratospheric ozone and cloud at this latitude are 0.3–0.4 % year^{-1} (averaged over 1979–2008) (Herman, 2010). For the shorter period measured here it is not possible to detect changes of that magnitude, and local effects on cloud could determine the magnitude (and sign) of the observed trend.

4.3 Ozone column dependence

The dependence of $J(O^1D)$ on solar zenith angle has been determined by sorting all data into 5° bins, and the results are summarized in Fig. 5. For this plot, zenith angles up to 82.5° have been included. All measurements have been adjusted to 1 a.u. (correction for the annual variation in the earth-sun distance; Iqbal, 1983). A few measurements made at solar zenith angles below 17.5° have been excluded as they represent a brief period in mid-summer. Included in the plot are $J(O^1D)$ estimates calculated using the TUV model for cloud free conditions and an aerosol optical depth

ACPD
14, 18389–18419, 2014

of 0.05. Calculations for two ozone column amounts are shown, 250 and 350 DU, which are typical seasonal maximum and minimum values observed in this location as derived from satellite measurements (TOMS) (http://disc.sci.gsfc.nasa.gov/acdisc/TOMS).

A significant fraction of the variability can be due to the differences in the ozone column during the year. To characterize the dependence, the measured $J(O^1D)$ values were fitted to a function of the form:

$$J(O^1D) = \left(\sum_i A_i \exp(-B_i/\cos\theta) \right) \cdot \left(O_3^{sat}/300\right)^{-RAF} \quad (8)$$

where θ is the solar zenith angle, O_3^{sat} is the total ozone column retrieved from satellite for the measurement day, and A_i, B_i and RAF are fitted. RAF is the Radiation Amplification Factor to be determined (Micheletti et al., 2003). The results for the fit to the entire dataset using either one or two exponential terms (i = 1 or 2) are shown in Table 2 and for one exponential term in Fig. 5. Using two exponentials produces a slightly better fit, and both fits produce an RAF estimate in excellent agreement with calculations of 1.4–1.5 (McKenzie et al., 2011).

Using this derived ozone RAF the dataset was normalized to both 300 DU and 1 a.u. as shown in Fig. 6. Given the large difference between the median and average values for the bins, a second fit was performed to the median of the binned values of Fig. 6, and the fits are also included in Table 2. For reference, the fits with two exponential terms, using all data and the medians is included in Fig. 6. It should be noted that the increase in R^2 is due to the change in the nature of the data being fitted.

The removal of the variation due to changes in stratospheric ozone, as described by the satellite ozone measurements, reduces the interquartile variability by up to 20 % as shown in Fig. 7. The effect on high sun (low solar zenith angle) measurements is smaller, as this is only collected in mid-summer and so the ozone variability is small. At higher solar zenith angles ($> 50^\circ$) the percentage reduction diminishes also, presumably because, as the absolute intensity decreases, other effects, including the impact of measurement uncertainty, become larger.

ACPD
14, 18389–18419, 2014

4.4 Cloud impact

Clouds can both reduce and enhance solar radiation at the ground level. Figure 6 shows that the 90th percentile value closely follows the clear-sky calculated value at solar zenith angles less than 50°. This implies that approximately 10 % of these measurements show an enhancement of radiation due to cloud, a phenomenon often observed (Calbó et al., 2005). The likelihood of this cloud enhancement appears to increase with increasing solar zenith angle with up to 25 % of measurements showing an enhancement by 65°, presumably as a result of the changes in scattering geometry in the atmosphere.

To assess the overall impact of cloud, the ratio of the median value to the calculated clear – sky value was determined (Fig. 8). This shows that for solar zenith angles greater than 70° the median is approximately 85 % of the calculated clear sky value. From 20–70° the calculated impact of cloud on $J(O^1D)$ increases by 5–6 %, a trend also predicted in models of the cloud impact on UV irradiance (Lindfors and Arola, 2008).

The results for solar zenith angles greater than 70° show that clouds have a diminishing impact as the sun approaches the horizon, as noted at other locations (Mateos et al., 2014). This can be a result of the increasing importance of scattered light under these conditions due to the longer atmospheric path for the direct beam. As scattered radiation has become more significant, it could be expected that clouds more readily enhance the observed radiation (Fig. 6) to the point that their overall impact is small (Fig. 8). However, both measurement uncertainties (smaller signals and variations in detector angular response) and modelling limitations could be playing a significant role. The enhancement in inter-quartile range, also shown in Fig. 8, could also be due to a combination of cloud impact or measurement uncertainty.

Attempts to capture the cloud variability through independent observations have not been very successful. Measures such as visual observations and automatic sky cameras have not been implemented at Cape Grim. While sunphotometers make measurements during this period, they do not make measurements of cloud optical depth as has

ACPD
14, 18389–18419, 2014

been used elsewhere (Anton et al., 2012). Longwave downward radiation (LDR) measurements have been used to estimate cloudiness (Marty and Philipona, 2000; Dürr and Philipona, 2004). The attraction of this measure is that LDR is relatively insensitive to the solar position, and so should be independent of the other factors influencing $J(O^1D)$. An attempt at using LDR has been made using half-hourly long-wave radiation averaged values measured at Cape Grim (Wilson and Shinkfield, 2007) to derive the Clear-Sky Index (Marty and Philipona, 2000). In this case it was possible to produce a fit extending Eq. (8) with an additional term (Clear-Sky Index)$^{\alpha}$, where α is a fitted parameter. Fitting the entire dataset where LDR values were available returned a significant value for the exponent (-0.19 ± 0.01). However, the fit did not improve significantly, as measured by the reduced R^2 (increases of ~ 0.0005). This could be due the insensitivity of long-wave radiation measures to higher-level clouds (Schade et al., 2009; Boers et al., 2010). However, cloud bases are often low at Cape Grim, as highlighted by LIDAR measurements, (Young, 2007) and so LDR should be a reasonable measure. It is more likely that the features of clouds that cause changes in the observed LDR are not simply related to those features which result in a significant reduction (or enhancement) of $J(O^1D)$.

4.5 Wider relevance of the observations

The atmospheric composition at Cape Grim is dependent on wind direction and clean or "baseline" conditions are defined by standard measures (Downey, 2007). The chemical outcome of the photolysis measured here will depend on whether the local atmosphere is clean or polluted. However, an analysis of the data presented here filtered for only those measurements collected under "baseline" conditions gives results not statistically different from those observed for the entire dataset. As the baseline selection process eliminates a significant fraction of the data, the variability does increase.

Another important question is how reliably the climatology measured here is representative of a larger region. Cape Grim, sitting on the coast could have a cloud environment different to locations out to sea and inland. A study of the global irra-

ACPD
14, 18389–18419, 2014

diance at a number of locations concluded that Cape Grim experienced cloud conditions similar to the southern ocean in this area (Bishop et al., 1997), and a study of rainfall has shown that while rainfall varies when moving inland it is reasonably constant along the coast (Jasper and Downey, 1991). The ISCCP dataset (http://isccp.giss.nasa.gov/index.html) shows that cloud amount at this latitude band over the oceans is 80–90 %, with little dependence on longitude and without an obvious trend over the period 1984–2008. Therefore, the cloud impacts observed at Cape Grim should be representative of the marine environment at these latitudes.

Modelling studies (Liu et al., 2006) calculated that the impact of cloud on $J(O^1D)$ is around 8 % averaged throughout the troposphere, but that ground level impacts are larger, of the order of −20 %. The data presented here shows a slightly smaller impact of cloud on $J(O^1D)$ when using the median estimate, but close to identical to that calculated using the mean values for the individual sza bins. The reduction is half that often observed for global UV irradiance at the average cloud factor of 0.8 to 0.9, underlining the relative insensitivity of actinic flux to cloud (Calbó et al., 2005). This is a result of the relative importance of diffuse radiation to the photolysis rate, and the limited impact of cloud on total diffuse irradiance (Blumthaler et al., 1994).

The results of this study permit the prediction of $J(O^1D)$ in the current climate. The impact of stratospheric ozone recovery should be well described by our current understanding. However, it would be useful to estimate the likely impact of future changes in clouds properties on $J(O^1D)$. With the reasonable agreement between models and observations seen at Cape Grim there can be some confidence in their predictions. For the maritime environment investigated here the overall impact of cloud is relatively small (15–20 %) given the 80–90 % cloud cover. Any future climate changes would need to change the frequency of clouds significantly to alter $J(O^1D)$ greatly. Other changes, such as a change in cloud optical depth may be more significant. Verifying any such changes in $J(O^1D)$ will require ongoing observations.

ACPD
14, 18389–18419, 2014

5 Conclusions

Six years of estimates of $J(O^1D)$ are presented for a clean Southern Hemisphere marine site. The impact of solar zenith angle and total column ozone can be clearly seen and quantified and the stratospheric ozone dependence is in good agreement with radiation model estimates. The impact of cloud can also be characterized, with bounds on the impact of clouds determined as a function of solar zenith angle. However, attempts at modelling the impact of clouds using independent radiation measurements (Longwave Downward Radiation) produced significant fits that did not significantly improve the quality of the model. So while the impact of cloud can be quantified, a good proxy for this has proven elusive.

Acknowledgements. This work would not be possible without the ongoing dedication and support of the staff at the Cape Grim Baseline Air Pollution Station and the financial support provided for work at Cape Grim by the Bureau of Meteorology. The inspiration of the other scientists involved in the Cape Grim programme is also gratefully acknowledged.

References

Antón, M., Alados-Arboledas, L., Guerrero-Rascado, J. L., Costa, M. J., C Chiu, J., and Olmo, F. J.: Experimental and modeled UV erythemal irradiance under overcast conditions: the role of cloud optical depth, Atmos. Chem. Phys., 12, 11723–11732, doi:10.5194/acp-12-11723-2012, 2012. 18402

Bishop, J. K. B., Rossow, W. B., and Dutton, E. G.: Surface solar irradiance from the International Satellite Cloud Climatology Project 1983–1991, J. Geophys. Res., 102, 6883–6910, doi:10.1029/96jd03865, 1997. 18403

Blumthaler, M., Ambach, W., and Salzgeber, M.: Effects of cloudiness on global and diffuse UV irradiance in a high-mountain area, Theor. Appl. Climatol., 50, 23–30, 1994. 18403

Boers, R., de Haij, M. J., Wauben, W. M. F., Baltink, H. K., van Ulft, L. H., Savenije, M., and Long, C. N.: Optimized fractional cloudiness determination from five ground-based remote sensing techniques, J. Geophys. Res., 115, D24116, doi:10.1029/2010jd014661, 2010. 18402

ACPD
14, 18389–18419, 2014

Bohn, B., Kraus, A., Muller, M., and Hofzumahaus, A.: Measurement of atmospheric $O_3 \rightarrow O(^1D)$ photolysis frequencies using filterradiometry, J. Geophys. Res., 109, D10S90, doi:10.1029/2003JD004319, 2004. 18393

Bohn, B., Corlett, G. K., Gillmann, M., Sanghavi, S., Stange, G., Tensing, E., Vrekoussis, M., Bloss, W. J., Clapp, L. J., Kortner, M., Dorn, H.-P., Monks, P. S., Platt, U., Plass-Dülmer, C., Mihalopoulos, N., Heard, D. E., Clemitshaw, K. C., Meixner, F. X., Prevot, A. S. H., and Schmitt, R.: Photolysis frequency measurement techniques: results of a comparison within the ACCENT project, Atmos. Chem. Phys., 8, 5373–5391, doi:10.5194/acp-8-5373-2008, 2008. 18392, 18393, 18394

Cainey, J., Derek, N., and Krummel, P. (Eds.): Baseline Atmospheric Program 2005–2006, Australian Bureau of Meteorology and CSIRO Marine and Atmospheric Research, Melbourne, 2007. 18394, 18396

Calbó, J., Pagès, D., and González, J. A.: Empirical studies of cloud effects on UV radiation: a review, Rev. Geophys., 43, RG2002, doi:10.1029/2004rg000155, 2005. 18401, 18403

Chance, K. and Kurucz, R. L.: An improved high-resolution solar reference spectrum for earth's atmosphere measurements in the ultraviolet, visible, and near infrared, J. Quant. Spectrosc. Ra., 111, 1289–1295, doi:10.1016/j.jqsrt.2010.01.036, 2010. 18395, 18396, 18397

Creasey, D. J., Evans, G. E., Heard, D. E., and Lee, J. D.: Measurements of OH and HO_2 concentrations in the Southern Ocean marine boundary layer, J. Geophys. Res., 108, 4475, doi:10.1029/2002JD003206, 2003. 18394, 18397, 18412

Crutzen, P. J.: Photochemical reactions initiated by and influencing ozone in unpolluted tropospheric air, Tellus, 26, 47–57, 1974. 18390

Downey, A.: Meteorology/Climatology 2005–2006, in: Baseline Atmospheric Program 2005–2006, edited by: Cainey, J., Derek, N., and Krummel, P., Australian Bureau of Meteorology and CSIRO Marine and Atmospheric Research, Melbourne, 39–45, 2007. 18402

Dürr, B. and Philipona, R.: Automatic cloud amount detection by surface longwave downward radiation measurements, J. Geophys. Res., 109, D05201, doi:10.1029/2003JD004182, 2004. 18402

Edwards, G. D. and Monks, P. S.: Performance of a single-monochromator diode array spectroradiometer for the determination of actinic flux and atmospheric photolysis frequencies, J. Geophys. Res., 108, 8546, doi:10.1029/2002JD002844, 2003. 18394

ACPD
14, 18389–18419, 2014

Forgan, B. W.: Sunphotometer Calibration by the Ratio-Langley Method, in: Baseline Atmospheric Program 1986, edited by: Forgan, B. W. and Fraser, P. J., 22–26, Bureau of Meteorology and CSIRO Division of Atmospheric Research, Melbourne, 1988. 18395

Frederick, J. E., Manner, V. W., and Booth, C. R.: Interannual variability in solar ultraviolet irradiance over decadal time scales at latitude 55 deg South, Photoch. Photobio. Sci., 74, 771–779, 2001. 18399

Heard, D. E. and Pilling, M. J.: Measurement of OH and HO_2 in the troposphere, Chem. Rev., 103, 5163–5198, 2003. 18391

Herman, J. R.: Use of an improved radiation amplification factor to estimate the effect of total ozone changes on action spectrum weighted irradiances and an instrument response function, J. Geophys. Res., 115, D23119, doi:10.1029/2010jd014317, 2010. 18399

Hofzumahaus, A., Lefer, B. L., Monks, P. S., Hall, S. R., Kylling, A., Mayer, B., Shetter, R. E., Junkermann, W., Bais, A., Calvert, J. G., Cantrell, C. A., Madronich, S., Edwards, G. D., Kraus, A., Muller, M., Bohn, B., Schmitt, R., Johnston, P., McKenzie, R., Frost, G. J., Griffioen, E., Krol, M., Martin, T., Pfister, G., Roth, E. P., Ruggaber, A., Swartz, W. H., Lloyd, S. A., and Van Weele, M.: Photolysis frequency of O_3 to $O(^1D)$: measurements and modeling during the International Photolysis Frequency Measurement and Modeling Intercomparison (IPMMI), J. Geophys. Res., 109, D08S90, doi:10.1029/2003JD004333, 2004. 18392, 18393, 18394

Iqbal, M.: An Introduction to Solar Radiation, Academic Press, Toronto, 1983. 18399

Jäkel, E., Wendisch, M., and Lefer, B.: Parameterization of ozone photolysis frequency in the lower troposphere using data from photodiode array detector spectrometers, J. Atmos. Chem., 54, 67–87, doi:10.1007/s10874-006-9014-1, 2006. 18396

Jasper, J. D. and Downey, A. H.: Towards a Cape Grim Climatology, in: Baseline Atmospheric Program 1989, edited by: Wilson, S. R. and Gras, J. L., Bureau of Meteorology and the CSIRO Division of Atmospheric Research, Melbourne, 38–46, 1991. 18403

Junkermann, W., Platt, U., and Volz-Thomas, A.: A photoelectric detector for the measurement of photolysis frequencies of ozone and other atmospheric molecules, J. Atmos. Chem., 8, 203–227, 1989. 18392

Kazadzis, S., Topaloglou, C., Bais, A. F., Blumthaler, M., Balis, D., Kazantzidis, A., and Schallhart, B.: Actinic flux and O^1D photolysis frequencies retrieved from spectral measurements of irradiance at Thessaloniki, Greece, Atmos. Chem. Phys., 4, 2215–2226, doi:10.5194/acp-4-2215-2004, 2004. 18392, 18393

ACPD
14, 18389–18419, 2014

Kylling, A., Webb, A. R., Bais, A., Blumthaler, M., Schmitt, R., Thiel, S., Kazantzidis, A., Kift, R., Misslbeck, M., Schallhart, B., Schreder, J., Topaloglou, C., Kazadzis, S., and Rimmer, J.: Actinic flux determination from measurements of irradiance, J. Geophys. Res., 108, 4506, doi:10.1029/2002JD003236, 2003. 18392, 18393, 18396

Lindfors, A. and Arola, A.: On the wavelength-dependent attenuation of UV radiation by clouds, Geophys. Res. Lett., 35, L05806, doi:10.1029/2007GL032571, 2008. 18401

Liu, H., Crawford, J. H., Pierce, R. B., Norris, P., Platnick, S. E., Chen, G., Logan, J. A., Yantosca, R. M., Evans, M. J., Kittaka, C., Feng, Y., and Tie, X.: Radiative effect of clouds on tropospheric chemistry in a global three-dimensional chemical transport model, J. Geophys. Res., 111, D20303, doi:10.1029/2005JD006403, 2006. 18403

Madronich, S. and Flocke, S.: Theoretical Estimation of Biologically Effective UV Radiation at the Earth's Surface, in: Solar Ultraviolet Radiation-Modeling, Measurements and Effects, edited by: Zerefos, C. and Bais, A., NATO ASI Subseries 1, Vol. 52, Springer-Verlag, Berlin, 23–48, 1997. 18397, 18417

Malicet, J., Daumont, D., Charbonnier, J., Parisse, C., Chakir, A., and Brion, J.: Ozone UV spectroscopy. 2. Absorption cross-sections and temperature dependence, J. Atmos. Chem., 21, 263–273, 1995. 18396

Marty, C. and Philipona, R.: The clear-sky index to separate clear-sky from cloudy-sky situations in climate research, Geophys. Res. Lett., 27, 2649–2652, doi:10.1029/2000gl011743, 2000. 18402

Mateos, D., di Sarra, A., Bilbao, J., Meloni, D., Pace, G., de Miguel, A., and Casasanta, G.: Spectral attenuation of global and diffuse UV irradiance and actinic flux by clouds, Q. J. Roy. Meteor. Soc., doi:10.1002/qj.2341, 2014. 18401

McKenzie, R., Johnston, P., Hofzumahaus, A., Kraus, A., Madronich, S., Cantrell, C., Calvert, J., and Shetter, R.: Relationship between photolysis frequencies derived from spectroscopic measurements of actinic fluxes and irradiances during the IPMMI campaign, J. Geophys. Res.-Atmos., 107, ACH 1-1–ACH 1-16, doi:10.1029/2001JD000601, 2002. 18392, 18393, 18396

McKenzie, R. L., Aucamp, P. J., Bais, A. F., Björn, L. O., Ilyas, M., and Madronich, S.: Ozone depletion and climate change: impacts on UV radiation, Photoch. Photobio. Sci., 10, 182–198, doi:10.1039/C0PP90034F, 2011. 18400

ACPD
14, 18389–18419, 2014

Micheletti, M. I., Piacentini, R. D., and Madronich, S.: Sensitivity of biologically active UV radiation to stratospheric ozone changes: effects of action spectrum shape and wavelength range, Photochem. Photobiol., 78, 456–461, 2003. 18400

Monks, P. S., Carpenter, L. J., Penkett, S. A., Ayers, G. P., Gillett, R. W., Galbally, I. E., and Meyer, C. P.: Fundamental ozone photochemistry in the remote marine boundary layer: the SOAPEX experiment, measurement and theory, Atmos. Environ., 32, 3647–3664, 1998. 18394, 18397

Sander, S. P., Friedl, R. R., Golden, D. M., Kurylo, M. J., Moortgat, G. K., Keller-Rudek, H., Wine, P. H., Ravishankara, A. R., Kolb, C. E., Molina, M. J., Finlayson-Pitts, B. J., Huie, R. E., and Orkin, V. L.: Chemical kinetics and photochemical data for use in atmospheric studies, Evaluation Number 15, JPL Publication 06-2, Jet Propulsion Laboratory, Pasadena, 2006. 18391, 18396

Schade, N. H., Macke, A., Sandmann, H., and Stick, C.: Total and partial cloud amount detection during summer 2005 at Westerland (Sylt, Germany), Atmos. Chem. Phys., 9, 1143–1150, doi:10.5194/acp-9-1143-2009, 2009. 18402

Schallhart, B., Huber, A., and Blumthaler, M.: Semi-empirical method for the conversion of spectral UV global irradiance data into actinic flux, Atmos. Environ., 38, 4341–4346, 2004. 18392, 18393

Sommariva, R., Haggerstone, A.-L., Carpenter, L. J., Carslaw, N., Creasey, D. J., Heard, D. E., Lee, J. D., Lewis, A. C., Pilling, M. J., and Zádor, J.: OH and HO_2 chemistry in clean marine air during SOAPEX-2, Atmos. Chem. Phys., 4, 839–856, doi:10.5194/acp-4-839-2004, 2004. 18397

Webb, A. R., Kift, R., Thiel, S., and Blumthaler, M.: An empirical method for the conversion of spectral UV irradiance measurements to actinic flux data, Atmos. Environ., 36, 4397–4404, 2002. 18392, 18393

Wilson, S. R. and Forgan, B. W.: Aerosol optical depth at Cape Grim, Tasmania 1986–1999, J. Geophys. Res., 107, 4068, doi:10.1029/2001JD000398, 2002. 18396, 18397

Wilson, S. R. and Shinkfield, P.: Passive Solar Radiation, in: Baseline Atmospheric Program 2005–2006, edited by: Cainey, J. M., Derek, N., and Krummel, P. B., Australian Bureau of Meteorology and CSIRO Marine and Atmospheric Research, Melbourne, p. 98, 2007. 18402

Wilson, S. R.: The Cape Grim Scanning UV Spectrometer, in: Baseline Atmospheric Program 2003–2004, edited by: Cainey, J. M., Derek, N., and Krummel, P. B., Bureau of Meteorology/CSIRO Atmospheric Research, Melbourne, 9–16, 2006. 18395

ACPD
14, 18389–18419, 2014

Wilson, S. R.: Effect of Temperature on the Cape Grim UV-B Records, in: Baseline Atmospheric Program 2005–2006, edited by: Cainey, J. M., Derek, N., and Krummel, P. B., Australian Bureau of Meteorology and CSIRO Marine and Atmospheric Research, Melbourne, 25–30, 2007. 18395

Wilson, S. R. and Forgan, B. W.: In situ calibration technique for UV spectral radiometers, Appl. Optics, 34, 5475–5484, 1995. 18395

Ylianttila, L. and Schreder, J.: Temperature effects of PTFE diffusers, Opt. Mater., 27, 1811–1814, doi:10.1016/j.optmat.2004.11.008, 2005. 18395

Young, S. A.: Interpretation of the MiniLIDAR Data Recorded at Cape Grim 1998–2000, in: Baseline Atmospheric Program 2005–2006, edited by: Cainey, J. M., Derek, N., and Krummel, P. B. Australian Bureau of Meteorology and CSIRO Marine and Atmospheric Research, Melbourne, 15–24, 2007. 18402

ACPD
14, 18389–18419, 2014

Table 1. Monthly mean photolysis rate $J(O^1D)$. This is calculated using hourly averages for each of the 24 h in the day.

Month	Mean (std. deviation) $s^{-1} \times 10^{-6}$
1	11.77 (0.45)
2	10.02 (0.80)
3	6.27 (0.71)
4	3.34 (0.28)
5	1.86 (0.27)
6	0.95 (0.07)
7	1.02 (0.03)
8	1.77 (0.14)
9	3.49 (0.72)
10	5.60 (0.77)
11	9.01 (0.45)
12	11.54 (0.80)

ACPD
14, 18389–18419, 2014

Table 2. Results for fitting $J(O^1D)$ with the form shown in Eq. (8). Brackets [. . .] surround values that have been assumed in the fit. Uncertainties (in brackets) are standard errors in the last quoted figure of the fitted parameters. Units for A_1 and A_2 are s^{-1}. The "median fit" is a fit to the medians as shown in Fig. 6.

Fit	$A_1/10^{-4}$	B_1	$A_2/10^{-5}$	B_2	RAF	R^2
All data	1.869(8)	1.626(3)			1.454(9)	0.863
	5.2(2)	2.94(4)	2.8(1)	0.77(2)	1.477(9)	0.871
Medians	2.4(2)	1.78(8)			[1.454]	0.995
	4.5(3)	2.59(10)	1.8(4)	0.62(7)	[1.454]	1.000

ACPD
14, 18389–18419, 2014

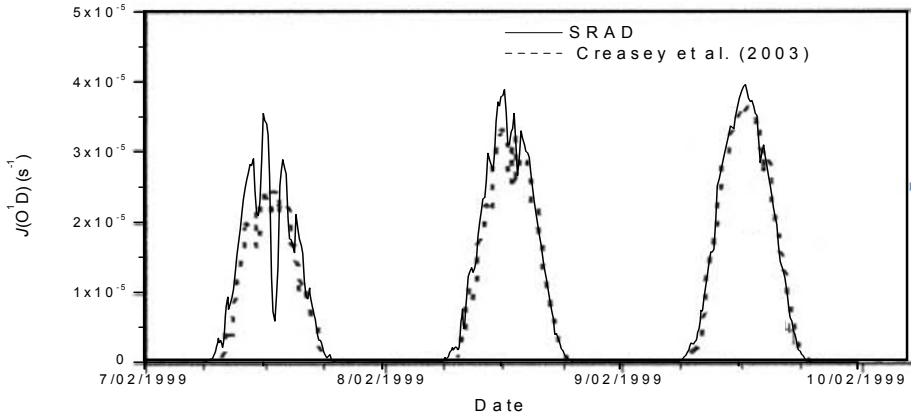

Figure 1. Comparison of SOAPEX-2 data (Creasey et al., 2003) and data derived from SRAD.

ACPD
14, 18389–18419, 2014

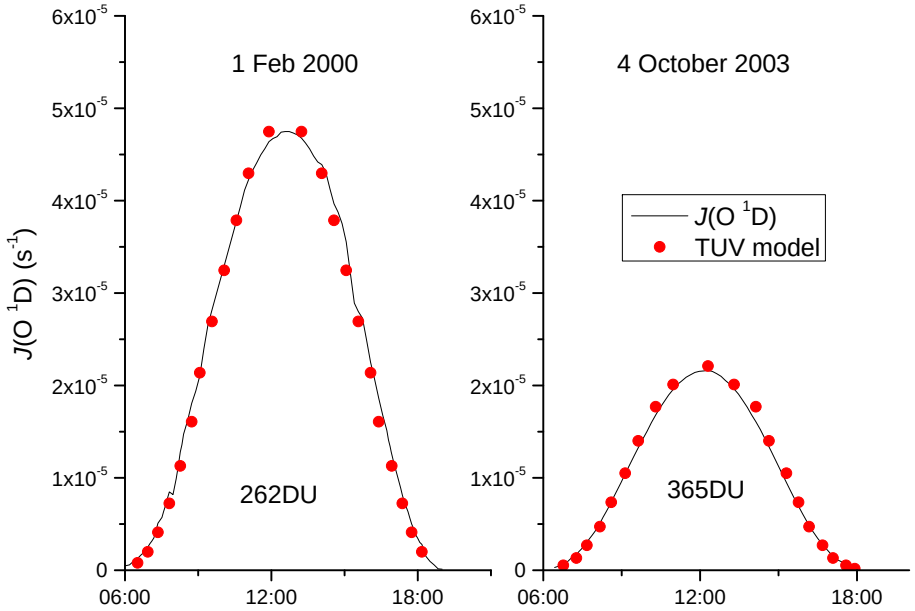

Figure 2. Comparison of clear sky calculation values to measurements. Calculations have been performed with the column ozone amount reported by satellite.

ACPD
14, 18389–18419, 2014

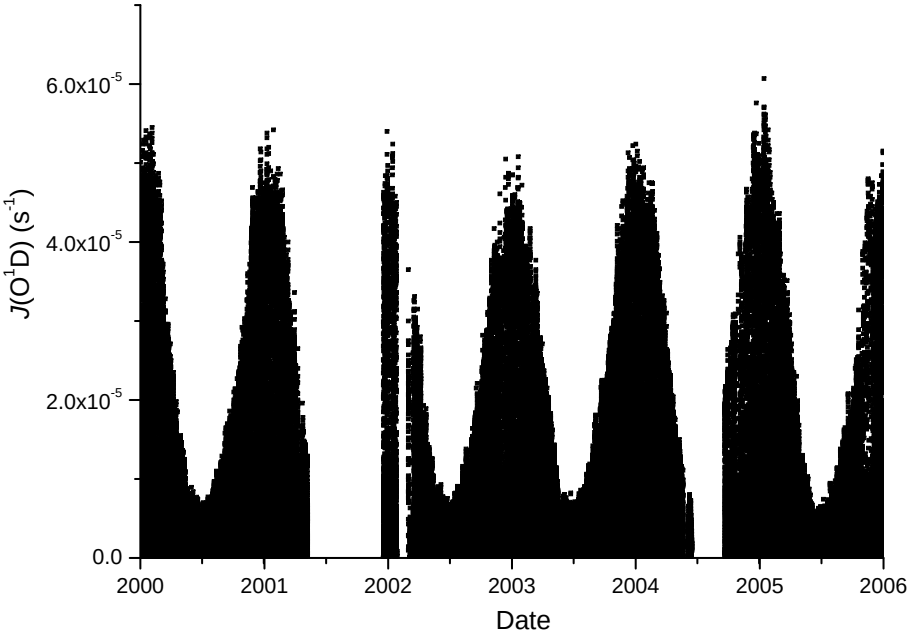

Figure 3. Photolysis rate $J(O^1D)$ observed at Cape Grim 2000–2005. Gaps in the data are due to instrument failure.

ACPD
14, 18389–18419, 2014

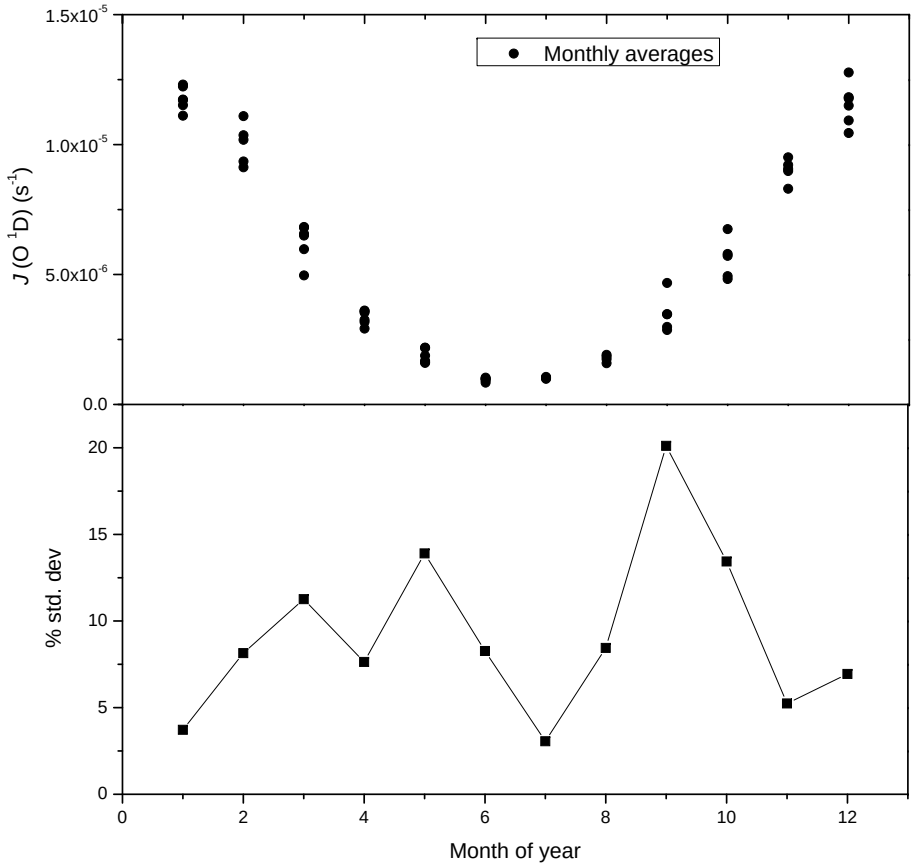

Figure 4. Annual cycle of $J(O^1D)$. The bottom panel shows the scatter in the monthly values as a percentage of the monthly mean.

ACPD
14, 18389–18419, 2014

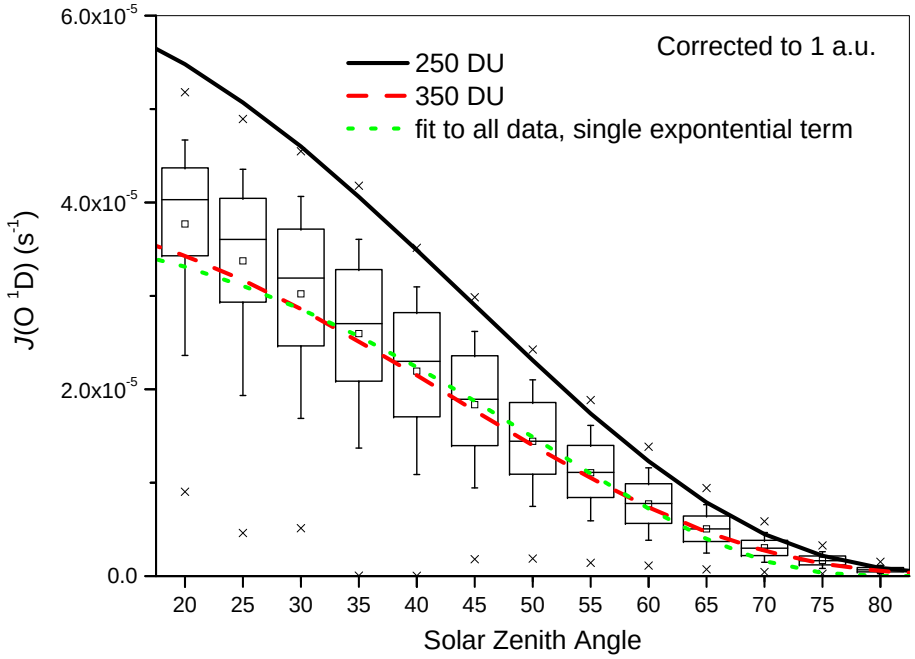

Figure 5. Solar zenith angle dependence of $J(O^1D)$. Crosses mark the 1 and 99 percentile. The boxes span 25/75 %, the whiskers mark 10 and 90 %, the central line indicates the median and the square the average value. The x axis value is the central value of the 5° bin used. The two solid lines were calculated using TUV (V 5.0) for ozone column amounts of 250 DU (February) and 350 DU (September). The dashed line is the fit to a single exponential term to all data.

ACPD
14, 18389–18419, 2014

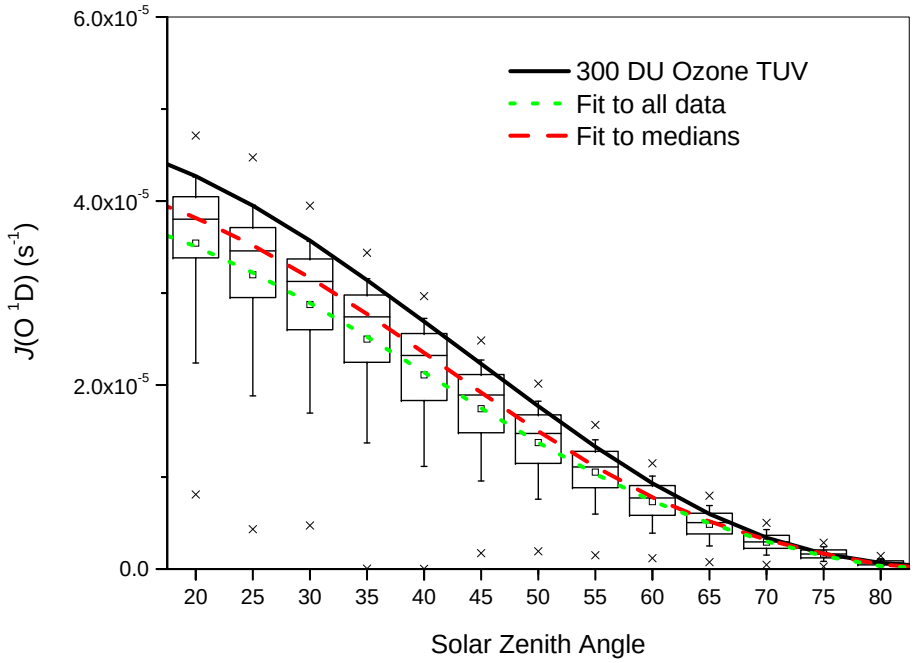

Figure 6. Cape Grim measurements of $J(O^1D)$ adjusted to a nominal 300 DU and 1 AU. The solid line is the calculated $J(O^1D)$ for clear skies and 300 DU ozone column and an aerosol optical depth of 0.05 using TUV 5.0 (Madronich and Flocke, 1997). The two broken lines are the results of the fits to two exponential terms to either all data or the median value of each bin (see also Table 2).

ACPD
14, 18389–18419, 2014

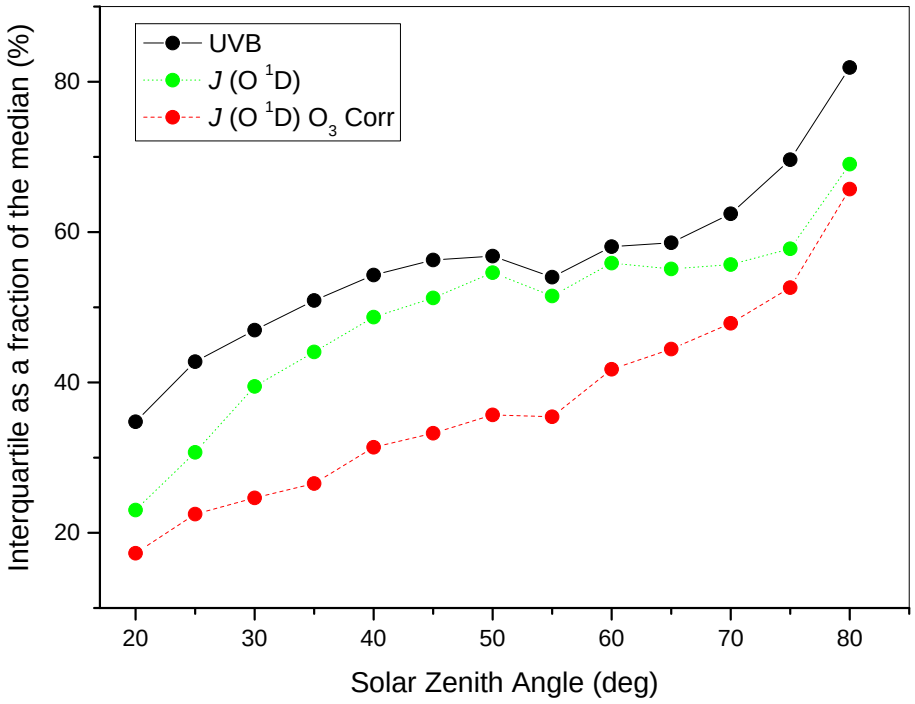

Figure 7. The interquartile (75–25 %) difference as a percentage of the median value as a function of solar zenith angle. UVB is the global irradiance, and the other two terms are the derived photolysis rates, with the red curve measurements have been corrected to a constant column ozone amount.

ACPD
14, 18389–18419, 2014

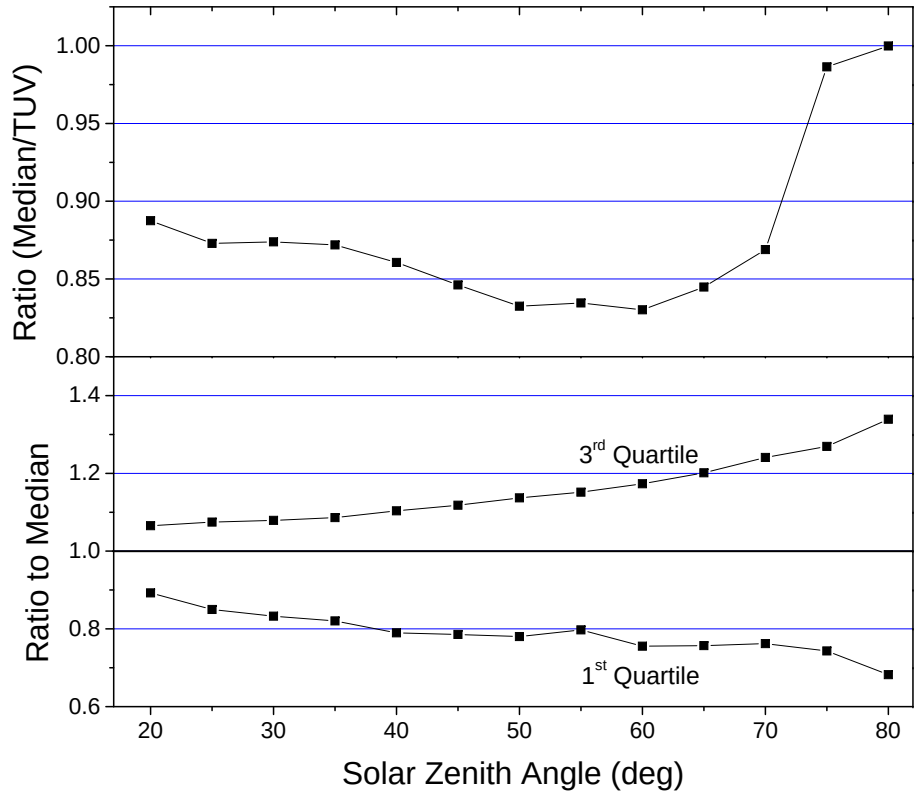

Figure 8. Top panel shows the ratio of the median measured $J(O^1D)$ to that from a calculation for clear skies. The bottom panel shows the spread in quartile values as a ratio to the median.

ACPD
14, 18389–18419, 2014